examining the past history of the turbulent flow and not by looking into its future motion.

Numerical Results

A collection of particle paths with which to evaluate the terms in Eq. (4) was obtained from a direct numerical simulation of turbulent channel flow[11] at Reynolds number $R^* = 173.2$ based on friction velocity and half-channel width. From initial locations on each of the planes $y^+ = 15.8$ and 37.5, 801 particles were followed forward in time. The total elapsed time of the simulation was $T^+ = 10$, which required 280 time steps to achieve. In the present discussion, y^+, T^+, and τ^+ refer to quantities scaled by wall variables. Each of the 280 calculated velocity fields was stored on magnetic tape so that backward paths could be computed. In this case, 601 particles were followed backward in time from each of the same two starting planes at $y^+ = 15.8$ and 37.5.

Ten randomly selected particles were followed forward and backward 280 time steps as a test of the accuracy of the computed paths. On average, the particles returned to within a very small distance, $d^+ \approx 0.44$, of their initial positions. Thus, the ensemble of computed paths appeared to be of sufficient accuracy to be used in the transport analysis. Additional details concerning the path data may be found in Ref. 12.

Figure 1 displays the normalized correlation functions R^*_{uu}, R^*_{vv}, and R^*_{ww} at $y^+ = 15.8$, while R^*_{uv} and R^*_{vu} are given in Fig. 2. The abscissa in all figures is taken as $-\tau^+$, so the curves to the left of the origin represent a backward analysis and those to the right a forward analysis. The curves for R^*_{vv} in Fig. 1 and R^*_{vu} in Fig. 2 are relevant to the evaluation of Eq. (4). For both positive and negative $-\tau^+$, R^*_{vv} falls relatively close to zero by $T^+ \approx 10$. On the other hand, only for $-\tau^+ < 0$ does R^*_{vu} approach zero. In fact, for $-\tau^+ > 0$, R^*_{vu} increases to values greater than one before eventually decreasing. This asymmetry is not unlike that observed in similar two-point Eulerian correlation functions.[13] It also complements the asymmetry of the gradient term in Eq. (4) mentioned previously. This is made clear in Fig. 3, which contains a plot of the computed terms in Eq. (4) normalized by $|\overline{uv}|$ at $\tau^+ = 0$. Note that at any time the four curves must sum to -1 and that the second term on the right-hand side of Eq. (4) is now given by $-R^*_{vu}$. For $-\tau^+ < 0$, the increase in $-R^*_{vu}$ from -1 toward zero coincides with a decrease in the gradient term; i.e., in the figure the gradient term decreases from 0 toward -1. The opposite effect occurs for $-\tau^+ > 0$, whererin the gradient term becomes positive while $-R^*_{vu}$ decreases below -1. This verifies that only a backward analysis of transport is useful.

The curve for Φ_2 in Fig. 3 is virtually zero for $|\tau^+| \leq 3$, strongly confirming the analysis leading to Eq. (3). For $|\tau^+| > 3$, second-order effects begin to mount. By $-\tau^+ \approx -10$, when $-R^*_{vu} \approx 0$, the normalized $\Phi_2 \approx 0.1$. Thus, the aforementioned requirement that a value of τ^+ exists for which the terms R_{vu} and Φ_2 are both small does not appear to be met. However, the 10% discrepancy to a gradient law introduced by the higher-order terms does not appear to be too serious.

It is seen in Fig. 3 that Φ_1 is a source of significant nongradient effects. At $-\tau^+ \approx -10$ its magnitude is 20% of the Reynolds stress. Since it has the same sign as Φ_2, the influence of these two sources of nongradient transport is additive. As a result, a purely gradient transport law appears to be in error by approximately 30% at $y^+ = 15.8$. Very similar trends to those shown in Figs. 1-3 were observed at $y^+ = 37.5$, though in this case the total simulation time was not long enough to bring R^*_{vu} as close to zero as it is in the $y^+ = 15.8$ case.

The present study reaffirms the need to develop Reynolds stress models that take into account important nongradient transport phenomena. One approach to this end is to work indirectly through vorticity transport modeling, where no pressure effects explicitly appear. Some preliminary steps in this direction have been taken[9] in which a Lagrangian analysis has been employed. A test of these results using particle path data as used in the present study is planned.

Acknowledgments

Support of P. S. Bernard for this study was provided in part through an American Society for Engineering Education/ Navy Summer Faculty Research Fellowship.

References

[1]Reynolds, W. C., "Computation of Turbulent Flows," *Annual Review of Fluid Mechanics*, Vol. 8, 1976, pp. 183-208.

[2]Taylor, G. I., "Eddy Motion in the Atmosphere," *Philosophical Transactions of the Royal Society*, Vol. 215, 1915, pp. 1-26.

[3]Taylor, G. I., "The Transport of Vorticity and Heat Through Fluids in Turbulent Motion," *Proceedings of the Royal Society*, Vol. 135A, 1932, pp. 685-705.

[4]Corrsin, S., "Limitations of Gradient Transport Models in Random Walks and Turbulence," *Advances in Geophysics*, Vol. 18A, 1974, pp. 25-60.

[5]Tennekes, J. and Lumley, J. L., *A First Course in Turbulence*, MIT, Cambridge, MA, 1972.

[6]Lakshminarayama, B., "Turbulence Modeling For Complex Shear Flows," *AIAA Journal*, Vol. 24, Dec. 1986, pp. 1900-1917.

[7]Hinze, J. O., *Turbulence*, 2nd ed., McGraw-Hill, New York, 1975, p. 580.

[8]Bernard, P. S. and Berger B. S., "A Method for Computing Three-Dimensional Turbulent Flows," *SIAM Journal on Applied Mathematics*, Vol. 42, June 1982, pp. 453-470.

[9]Bernard, P. S., "Non-Gradient Transport Phenomena in Turbulent Shear Flows," *Proceedings First National Fluid Dynamics Congress*, AIAA, Washington, DC, 1988, pp. 553-557 (AIAA Paper 88-3749-CP).

[10]Rhines, P. B. and Holland, W. R., "A Theoretical Discussion of Eddy-Driven Mean Flows," *Dynamics of Atmospheres of Oceans*, Vol. 3, July 1979, pp. 289-325.

[11]Hansen, R. J., Handler, R. A., Leighton, R. I., and Orszag, S. A., "Prediction of Turbulence-Induced Forces on Structures from Full Numerical Solutions of the Navier-Stokes Equations," *Journal of Fluids and Structures*, Vol. 1, Oct. 1987, pp. 431-443.

[12]Bernard, P. S., Ashmawey, M F., and Handler, R. A., "An Analysis of Particle Trajectories in Computer Simulated Turbulent Channel Flow," *Proceedings of the Eleventh Symposium on Turbulence,* Univ. Missouri, Rolla, MO, 1988.

[13]Antonia, R. A. and Van Atta, C. W., "Statistical Characteristics of Reynolds Stresses in a Turbulent Boundary Layer," *AIAA Journal*, Vol. 15, Jan. 1977, pp. 71-75.

Steady, Shock-Capturing Method Applied to One-Dimensional Nozzle Flow

S. Parameswaran*
Texas Tech University, Lubbock, Texas

Introduction

UPWIND difference schemes are becoming increasingly popular for the solution of the Euler equations because they are compatible with the characteristic theory (see Refs. 1-3). In the present method, the steady Euler equations are modeled by an upwind difference scheme and solved by a modified version of the SIMPLE algorithm originally developed for steady, incompressible flows by Patankar and Spalding.[4]

Received March 22, 1988; revision received Dec. 20, 1988.

*Visiting Assistant Professor, Department of Mechanical Engineering.

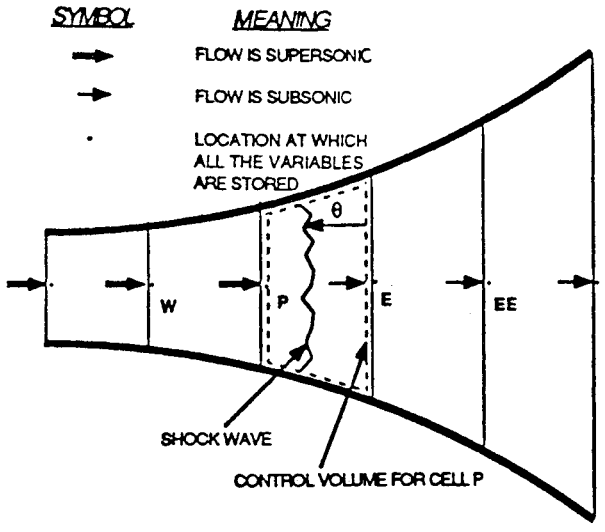

Fig. 1 Finite-volume cells for the one-dimensional nozzle.

The present method has many similarities to the one proposed by Wornom and Hafez.[5] However, in the present method all three conservation laws are satisfied within a "shock cell" (where the flow goes from supersonic to subsonic) by adjusting the shock position inside the cell. The novelty of the present approach is that it can locate the shock position accurately within two mesh points without imposing the Rankine-Hugoniot relationships across the shock.

In the present work, the steady, inviscid, quasi-one-dimensional flow of a perfect gas through a duct of variable cross-sectional area $a(x)$ is considered. The transport equations that govern the conservation of mass, momentum, and energy of inviscid, quasi-one-dimensional flows without any heat transfer can be expressed as follows:

$$\frac{\partial}{\partial x}(\rho u a) = 0 \tag{1a}$$

$$\frac{\partial}{\partial x}(\rho u^2 a) = -a\frac{\partial p}{\partial x} \tag{1b}$$

$$\frac{\partial}{\partial x}(e + p/\rho + u^2/2) = 0 \tag{1c}$$

where a, ρ, u, e, and p are, respectively, the area, density, velocity, specific internal energy, and pressure. For simplicity, the equation of state is chosen to be that of a perfect gas as follows:

$$p = (\gamma - 1)\rho e \tag{2}$$

where γ is the ratio of the specific heats for the perfect gas.

Figure 1 shows a typical one-dimensional nozzle, divided into several finite-volume cells. All the flow variables, such as velocity, pressure, density, etc., are stored at the cell node P, as shown in Fig. 1. In general, there *may* be a shock inside a cell and this is monitored by variable θ, which is the ratio of the distance of the shock from the east face of the cell to the cell width. From the definition, θ can assume values only between 0 and 1. The present method exploits this restriction on θ to locate the shock accurately within a cell width. The finite-volume equations describing the flow are considered next.

Difference equations are derived for the variables stored at grid node P, by integrating the transport Eqs. (1) over the control volume shown in Fig. 1. The finite-volume equations describing the conservation of mass, momentum, and energy for the control volume are given below:

$$\rho_P u_P a_P = \rho_E u_E a_E \tag{3}$$

$$\rho_P u_P a_P (u_E - u_P) = [\theta a_P + (1-\theta)a_E](p_P - p_E) \tag{4}$$

$$e_P + \rho_P/\rho_P + u^2{}_P/2 = h_0 \tag{5}$$

The equation of state is expressed as follows:

$$\rho_P = \rho_P(\gamma - 1)e_P \tag{6}$$

where γ is the specific heat ratio for a perfect gas and h_o is the total enthalpy of the flow that remains constant in the present study. Note that the continuity condition is implicitly assumed in the momentum equations, and for a "general" cell, where the flow is continuous, θ takes the value of 0.5. For a cell where there is a normal shock, θ is assigned to the value of shock position from the east face of the cell.

The coupled, nonlinear, finite-difference equations (3-6) are solved by the following five-step iterative procedure.

1) The pressure field is guessed and the corresponding velocity field u^* is obtained from Eq. (4) as follows:

$$\rho^n_p u^n_p a_P (u^*_E - u^*_P) = [\theta a_P + (1-\theta)a_E](p^n_p - p^n_E) \tag{7}$$

where superscript n indicates that the variable is obtained from the previous iteration.

2) The predicted u^* field is employed in Eq. (5) to obtain the e^* field. From the state equation, the new density field ρ^* is obtained.

3) Since a guessed pressure field is employed in the above calculations, in general, the continuity equation (3) may not be satisfied. Hence, there will be a continuity error associated with each cell, given by:

$$\mathcal{E}^*_P = \rho^*_P u^*_P a_P - \rho^*{}_E u_E a_E \tag{8}$$

4) Pressures are adjusted to eliminate the continuity error $\mathcal{E}^*$. For the cell, where there is a normal shock, i.e., inlet is supersonic and outlet is subsonic, the value of θ is adjusted to eliminate the continuity error for that cell.

5) Steps 1-4 are repeated until the continuity error in all the cells is sufficiently low *and* the value of θ obtained for the cell with the normal shock lies between 0 and 1.

The adjustments made to p and θ in step 4 depend on the local flow conditions and are crucial to the success of the method. These adjustments depend on the type of the cell, which is classified as follows:

a) inlet and exit velocities at the cell faces are supersonic (FLTYPE = 1);

b) inlet and exit velocities at the cell faces are subsonic (FLTYPE = 2);

c) flow is subsonic at inlet face and supersonic at outlet face (FLTYPE = 3);

d) flow is supersonic at inlet face and subsonic at outlet face (FLTYPE = 4).

Pressures at different locations are adjusted for those cells with FLTYPE values of 1 to 3. The pressure adjustment procedure for the first three types of cells are fully described in Ref. 6. Hence, only the correction equations for pressure are given in Table 1 for these cells.

If cell P contains a normal shock, i.e., the value of FLTYPE is 4, then the shock position inside the cell is adjusted to eliminate the continuity error. This is the main contribution of the present work and is described next.

Figure 1 shows a cell of FLTYPE = 4, i.e., the flow goes from supersonic to subsonic inside the cell. This is a special cell because the pressure at P is adjusted to eliminate the continuity error of the cell west of P; the pressure of E is adjusted to eliminate the continuity error of the cell east of P. Hence, for cell P, the continuity error remains unchanged. This is eliminated by adjusting the shock position θ within the cell. From the momentum equation, (7), it is clear that a change in the shock position θ will produce a change in the velocity at E. Hence, for this cell, the shock position is adjusted to eliminate the continuity error. The necessary correction in the shock position θ to eliminate the continuity error in the P cell is given by:

$$\theta' = \mathcal{E}^*/A_\theta \tag{12}$$

Table 1 Flow types and pressure correction equations

FLTYPE	Adjusted pressure node	Correction equation
1 $M_P>1$ and $M_E>1$	E	$p'_E(M_E^2-1)a_E/u_E=\varepsilon^*$, Eq. (9)
2 $M_P<1$ and $M_E<1$	P	$p'_P1-M_P^2)a_P/u_P=\varepsilon^*$, Eq. (10)
3 $M_P<1$ and $M_E<1$	P	$p'_P=0.5^*(p'_N+p'_E)$, Eq. (11)

where,

$$A_\theta=a_E\rho_E(a_P-a_E)(p_P-p_E)[1+(\gamma-1)M_E^2]/(a_P\rho_P u_P)$$

After the correction, if $\theta>1$, the normal shock is moved into the west cell; if $\theta<0$, it is moved into the east cell. If the value of θ is between 0 and 1, the shock remains in the P cell. The process of static pressure correction and θ correction is continued until the continuity error in *all* cells is sufficiently low. Other computational details are briefly described in the following paragraphs.

Boundary Condition

At inlet, the total pressure and total temperature are prescribed regardless of the Mach number. If the flow is subsonic at inlet, no other condition is imposed at inlet; at exit, the static pressure is given if the flow is subsonic there. On the other hand, if the flow is supersonic at inlet, the static pressure is prescribed there; at exit, no condition is imposed if the flow is supersonic there.

Initial Conditions

The static pressures at all nodes are guessed. Normally this is done by assuming a uniform pressure gradient between inlet and exit. If either the inlet or the exit pressure is not given, it is also guessed, normally, as a percentage of the total pressure.

Convergence

The solution is assumed to be converged when the value of *normalized continuity error* (continuity error divided by mass flow rate) for any cell is lower than 10^{-4}.

Relaxation of Pressure Correction and "θ Correction"

The corrections obtained for pressure and shock postion are always underrelaxed to avoid any large changes as follows:

$$p_{\text{new}}=p^*+\text{RELP}^*p' \qquad \theta_{\text{new}}=\theta^*+\text{RELT}^*\theta' \tag{13}$$

In the present study, RELP and RELT are assigned 0.6 and 0.5, respectively.

Below, the computational results obtained for two model problems are presented and compared with the analytical solution.

Divergent Duct

In the model problem considered by Shubin et al.[7], the flow goes through a shock from supersonic to subsonic in a one-dimensional divergent duct. The duct cross-sectional area $a(x)$ is given by:

$$a(x)=1.398+0.347^*\tanh(0.8^*\times-4) \tag{14}$$

At inlet $x=0$, following conditions were specified:

$$a_{\text{in}}=1.050,\quad p_{\text{in}}=0.502,\quad e_{\text{in}}=1.897,\quad u_{\text{in}}=1.299 \tag{15}$$

At outlet, ($x=10$), the static pressure was fixed as follows:

$$p_{\text{out}}=0.748 \qquad a_{\text{out}}=1.745 \tag{16}$$

Numerical predictions were obtained for two different mesh points, $N=17$ and 31. For this problem, an exact solution can be computed and in this exact solution a shock stands at $a=1.347$. Excellent agreement is obtained between the numerical predictions and the analytical solution for both grid systems. From the value of θ for the shock cell, the shock position can be calculated quite accurately. With the aid of 17 and 31 mesh points, the computed shock stands, respectively, at $a=1.350$ and 1.347 ($a_{\text{exact}}=1.347$).

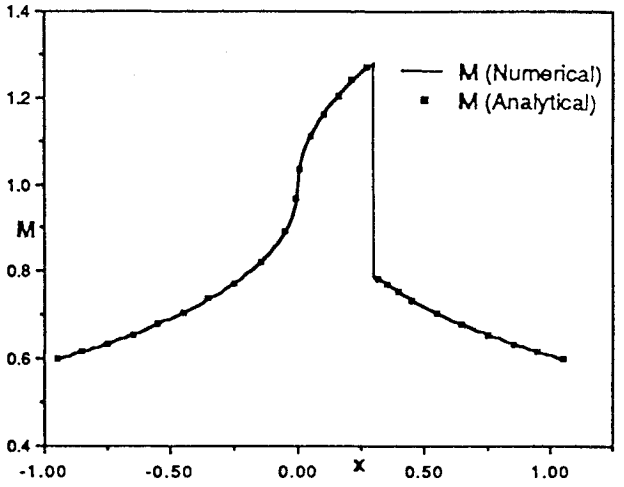

Fig. 2 Convergent-divergent duct; comparison of numerical prediction with analytical solution for Mach number ($N=28$).

Convergent-Divergent Duct

The results obtained for a convergent-divergent duct similar to the one considered by Van Hove and Arts[8] are presented below. For this case, the flow goes from subsonic to supersonic and then becomes subsonic through a shock. The duct cross-sectional area $a(x)$ is given below:

$$a(x)=1+0.2^*|x| \quad (-1<\times<1) \tag{17}$$

At inlet $x=0$, following conditions were specified:

$$a_{\text{in}}=1.21,\quad p_0=1.0,\quad h_0=3.5 \tag{18}$$

At outlet the static pressure was specified:

$$p_{\text{out}}=0.77 \tag{19}$$

For the above problem, an exact solution can be calculated, and in this exact solution the throat is choked and a shock stands at $a=1.06$. It is interesting to note that from the inlet conditions, the mass flow through the duct cannot be computed. Unlike Van Hove and Arts, no other boundary conditions are imposed except those specified by Eqs. (18) and (19). The mass flow through the duct was computed by the numerical procedure.

Numerical predictions obtained for Mach numbers with 27 mesh points are compared with the analytical solution in Fig. 2. It is clear that the agreement is excellent. From the predictions, the shock stands at $a=1.06$, which is in excellent agreement with the analytical shock position. The computed mass flow through the duct is 0.6848 and the analytical value of this is 0.6848.

Conclusion

A steady-state, shock-capturing procedure is developed for one-dimensional gas dynamic equations, and the method is

applied to two model problems. In both cases excellent agreement is obtained between numerical prediction and analytical solution. The method is also capable of locating the shock accurately within two mesh points. Extension of the methodology to two space dimensions on a streamline grid system has been completed, and the findings will be reported in the near future.

Acknowledgments

This work was performed at the Computational Fluid Dynamics Unit of the Imperial College, London, and was supported by a Commonwealth Scholarship. The author wishes to thank Professor Brian Spalding and Dr. George Carroll for their helpful discussions and enthusiasm.

References

[1]Wornom, S. F., "Implicit Conservative Characteristic Modeling Schemes for the Euler Equations—A New Approach," AIAA Paper 83-1935, July 1983.

[2]Chakravarthy, S. R., Anderson, D. A., and Salas, M. D., "The Split Coefficient Matrix Method for Hyperbolic Systems of Gas Dynamic Equations," AIAA Paper 80-0268, Jan. 1980.

[3]Steger, J. L. and Warming, R. F., "Flux Vector Splitting of the Inviscid Gasdynamic Equations with Applications to Finite Difference Methods," *Journal of Computational Physics,* Vol. 40, April 1981, pp. 263-293.

[4]Patankar, S. V. and Spalding, D. B., "A Calculation Procedure for Heat, Mass and Momentum Transfer in Three-Dimensional Parabolic Flows," *International Journal of Heat and Mass Transfer,* Vol. 15, March 1972, pp. 1787-1806.

[5]Wornom, S. F. and Hafez, M. M., "Implicit Conservative Schemes for the Euler Equations," *AIAA Journal,* Vol. 24, Feb. 1986, pp. 1215-223.

[6]Jennions, I. K., "The Impingement of Axisymmetric Supersonic Jets on Cones," Ph.D. Thesis, University of London, 1980.

[7]Shubin, G. R., Stephen, A. B., and Glaz, H. M., "Steady Shock Tracking and Newton's Method Applied to One-Dimensional Duct Flows," *Journal of Computational Physics,* Vol. 39, April 1981, pp. 364-374.

[8]Van Hove, G. A. and Arts, A., "Comparison of Several Finite Difference Schemes for Time Marching Methods Applied to One-Dimensional Nozzle Flow," von Kármán Institute for Fluid Dynamics, TN 132, Aug. 1979.

Inviscid, Unsteady, Transonic Axisymmetric Flow in Nozzles with Shock Waves

Carlos Frederico Estrada Alves*
CTA, Instituto de Atividades Espaciais, São José dos Campos, Brasil
and
Demétrio Bastos-Netto†
INPE, Instituto de Pesquisas Espaciais, São José dos Campos, Brasil

Introduction

KNOWLEDGE of the behavior of shock waves in unsteady transonic nozzle flow is important when investigating internal machinery flows. These transient conditions may occur because of combustion instabilities or changes in power settings, among other reasons.[1]

Two techniques have been used to handle this type of problem: similarity transformations[2,3] and asymptotic expansions.[1,4] In particular, Messiter and Adamson[4] discussed the case of a steady two-dimensional transonic flow and presented analytical results for an axisymmetric nozzle flow using the asymptotic technique. This Note reviews this analytical development of Messiter and Adamson[4] for the axisymmetric transonic flow and extends it to include unsteady conditions suggested by those authors and Richey.[3]

Governing Equations

Consider an unsteady, inviscid, transonic, axisymmetric chocked flow of a perfect gas as shown in Fig. 1. The governing equations can be obtained by imposing small perturbations in a steady, uniform, irrotational flowfield. Using the same nomenclature and procedure as Richey and Adamson,[1] one can make the flow velocity components $\bar{U}$ and $\bar{V}$ dimensionless with respect to the sonic speed $\bar{a}^*$. The longitudinal and radial coordinates $\bar{x}$ and $\bar{r}$ are normalized by $\bar{L}$ (the radius of the nozzle throat) and the time $\bar{T}$ by $\bar{L}/\bar{a}^*$.

Outer Region

The dimensionless velocity potential function,[1] $\Phi(x,r,t) \equiv \bar{\Phi}(\bar{x},\bar{r},\bar{t})/\bar{L}\bar{a}^*$, can be asymptotically expanded in terms of E (where E can be seen as the square root of the ratio between the throat radius and the radius of the nozzle curvature at the throat) and, together with the Bernouilli equation, substituted in the gasdynamic equation[1] for the velocity potential (as $U=\Phi_x$ and $V=\Phi_r$). From symmetry, $V=0$ at $r=0$.

The wall profile[3] can be taken as $r_w=[1+E^2f(x,t)]$, where $f(0,t)=0$. The boundary conditions,[4] assuming stationary walls [$f=f(x)$ only] can be written as

$$\phi_{2r}|_{r=1}=f' \tag{1a}$$

$$\phi_{3r}|_{r=1}=\phi_{1x}\phi_{2r}|_{r=1} \tag{1b}$$

where subscripts x and r mean $\partial/\partial x$ and $\partial/\partial r$, respectively, the numbered subscripts designate the expansion order, and $f'=df/dx$.

Further, to first order, $\phi_1=\phi_1(x,t)$ only and from the second-order term, together with Eq. (1a), one can write the first-order governing equations as

$$\frac{2k}{\gamma+1}\phi_{1xt}+\phi_{1x}\phi_{1xx}=\frac{2f'}{\gamma+1} \tag{2}$$

where γ is the specific heat ratio.

Substituting Eqs. (1b) and (2) into the third-order term[4] and integrating with respect to x, one obtains an equation for $h(x,t)$,

$$\left(\frac{3-2\gamma}{6}\right)\phi_{1x}^3+\frac{k}{4}\left(\frac{3-\gamma}{\gamma+1}\right)\int_x(\phi_{1x}^2)_t\,dx$$
$$=f''\frac{\phi_{1x}}{4}+\frac{2k}{\gamma+1}h_t+k\left(\frac{\gamma-1}{\gamma+1}\right)\phi_{1x}\phi_{1t}$$
$$+\phi_{1x}h_x+A_1(t) \tag{3}$$

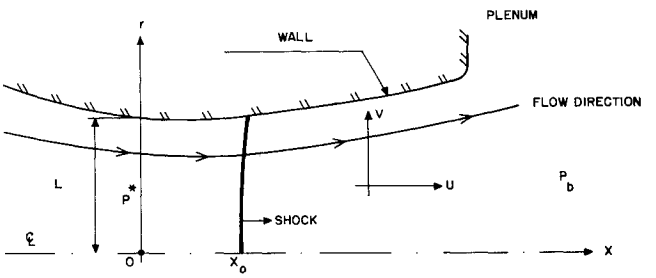

Fig. 1 Suggested nozzle flow geometry.

Received Sept. 9, 1987; revision received Aug. 31, 1988.

*Assistant Researcher.
†Senior Researcher. Member AIAA.